MICROPARTICLE IMPACTS IN SPACE

RESULTS FROM SOLAR MAX SATELLITE AND SHUTTLE WITNESS PLATE INSPECTIONS

David S. McKay
NASA Lyndon B. Johnson Space Center
Mail Code SN14
Houston, TX 77058

The Solar Maximum Satellite developed electronic problems after operating successfully in space for several years. Astronauts on Space Shuttle mission STS-41C retrieved the satellite into the orbiter cargo bay, replaced defective components, and re-deployed the repaired satellite into orbit. The defective components were returned to Earth for study. Scientists in the Solar System Exploration Division at Johnson Space Center in Houston have been examining the space-exposed surfaces. The approach and objectives of these studies are shown in Figure 1.

MICROPARTICLE IMPACT ON RETURNED SOLAR MAXIMUM HARDWARE

Approach and Objectives:

1. Document morphology of impact.
2. Find and analyze projectile residue.
3. Classify impact by origin.
4. Determine flux distribution.
5. Determine implications for space exposure.

Figure 1

Figure 2 illustrates the geometry and positioning of the Attitude Control Systems Box as seen before recovery and repair of the satellite. Thermal blankets and louvers exposed to space were retrieved by Shuttle astronauts during Solar Max repair mission STS-41C. These louvers and blankets have been inspected by means of scanning electron microscopy in order to determine fluxes and origins of impacting projectiles.

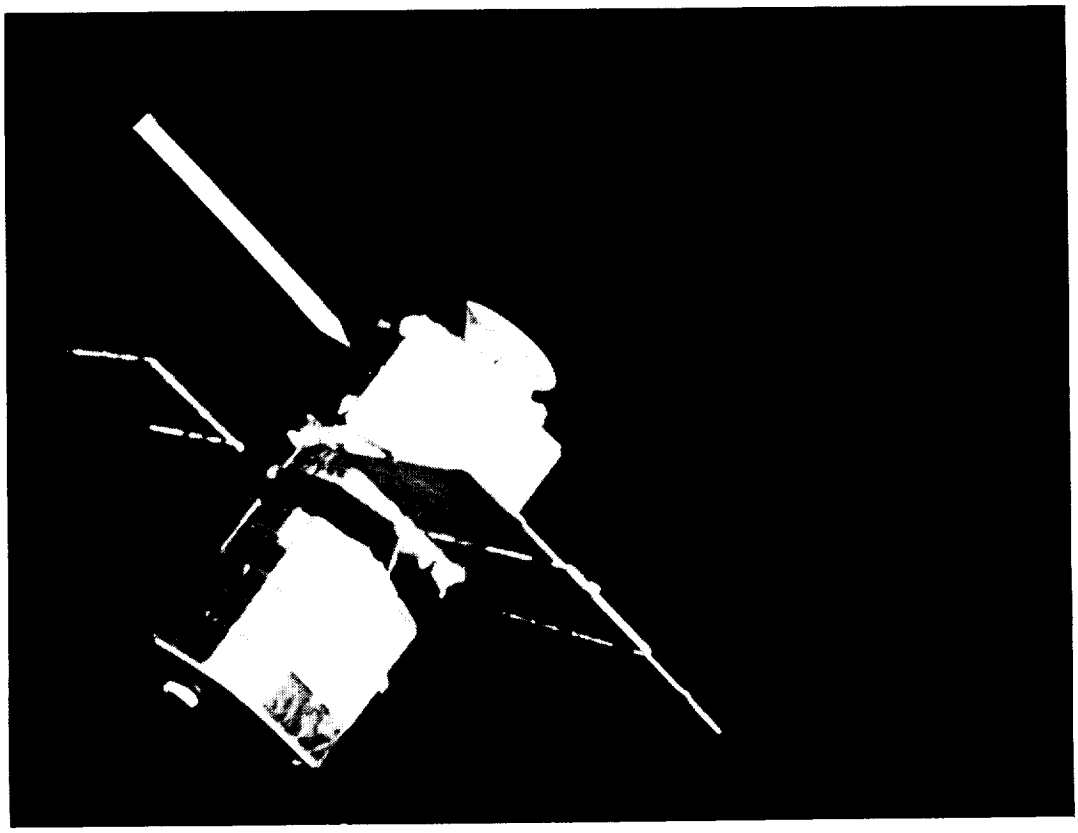

Attitude Control Systems Box before recovery and repair of satellite.

Figure 2

The Attitude Control Systems Box was returned from the Solar Maximum Satellite after spending 50 months in low-Earth orbit. One side of this box contained 84 aluminum thermal control louvers. These louvers had been penetrated by 64 impacts which made holes ranging from 180 micrometers to 820 micrometers in diameter. The location of these holes is shown in Figure 3. Most of these holes were made by micrometeorites as identified by chemical analysis of projectile residue associated with each hole. Micrometeorite holes are shown by open circles in this Figure. Seven of the holes were made by small particles of orbital debris. These holes are shown as filled circles on Figure 3.

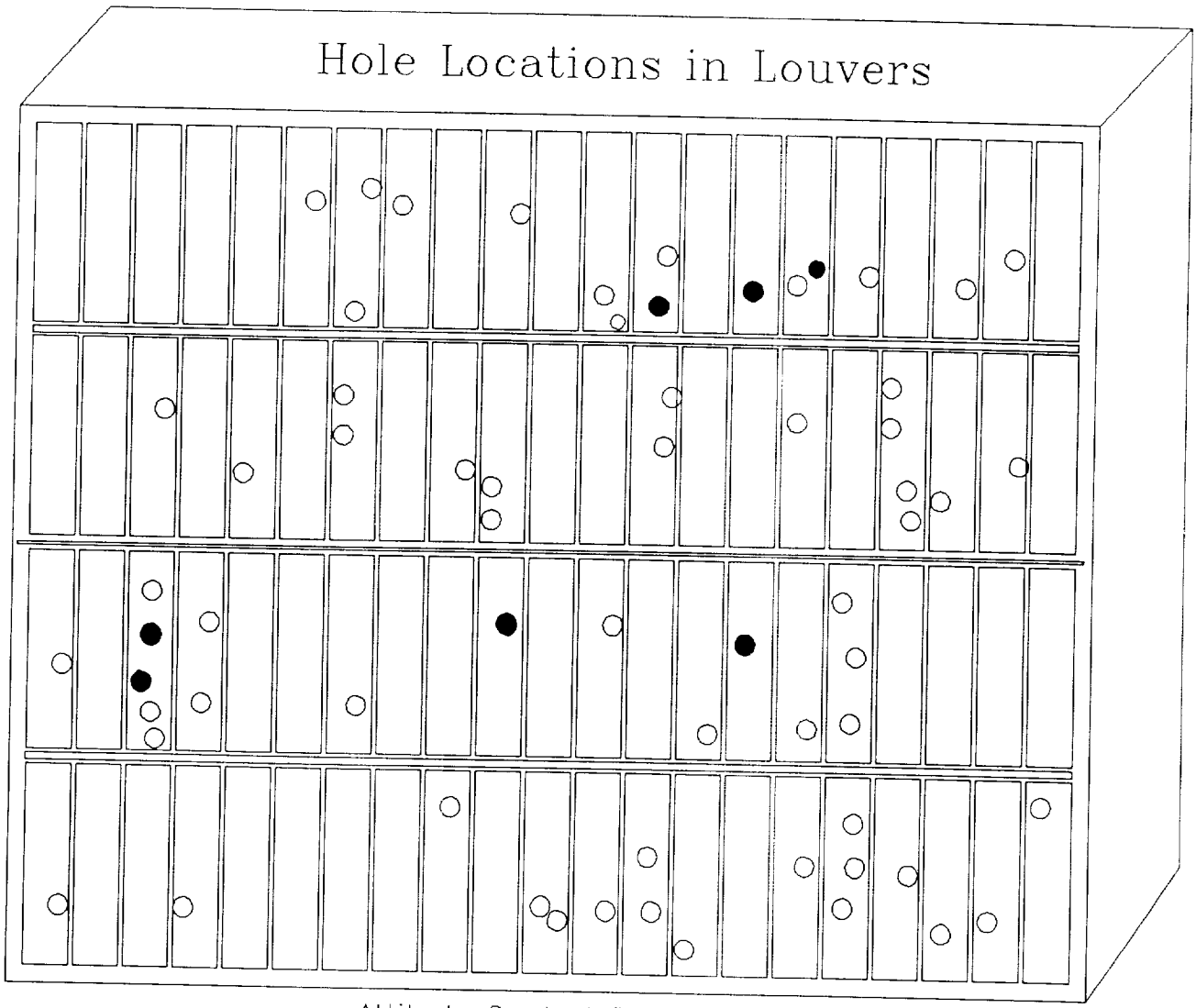

Figure 3

Figure 4 shows the structure of the aluminum louver and the morphology of a typical impact hole. The louver consists of two sheets of aluminum, each 125 micrometers thick, separated by a 3-millimeter space except at the edges and along a central support rib. A typical hypervelocity impact has three major morphologic features. The entry hole (Figure 4.1) is generally quite circular and has an upturned rim of aluminum which usually contains traces of residue from the projectile. The exit hole (Figure 4.2) also contains an overturned rim which is usually more jagged and less regular than the entry rim. All penetration holes are also associated with a spray pattern (Figure 4.3) on the second layer. This spray pattern is always much larger than the diameter of the hole, usually an order of magnitude larger in diameter and two orders of magnitude larger in area. The spray pattern is formed by the combined material from the projectile and the aluminum from the hole. Usually the aluminum from the hole is the primary constituent of the spray. The spray pattern consists of large numbers of small irregular craters which are sometimes arranged in loops and chains. Some of these small irregular craters on the second layer completely penetrate the aluminum layer, but most do not. Sometimes a secondary spray is created at the second layer which sprays tiny aluminum droplets back up to coat the bottom of the first layer (Figure 4.2) or which completely exit through the hole and create many more orbital debris microparticles in space.

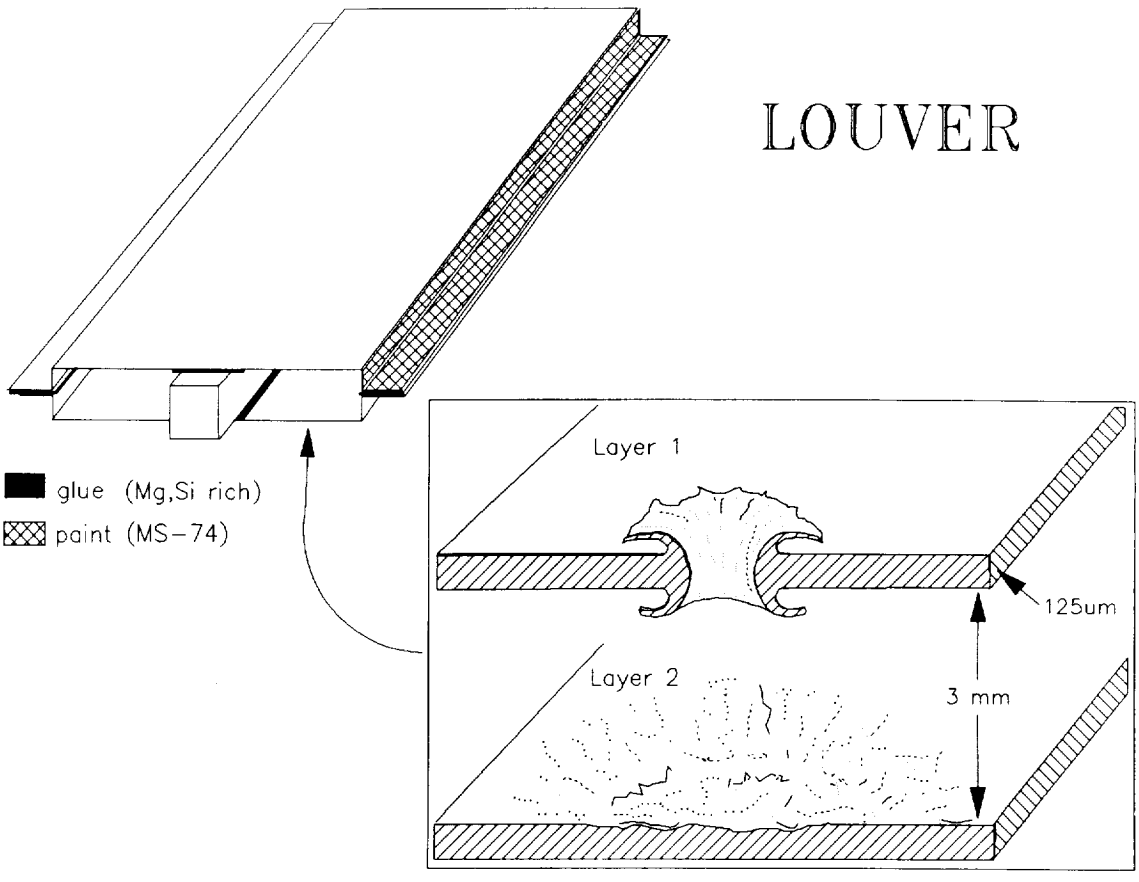

Figure 4

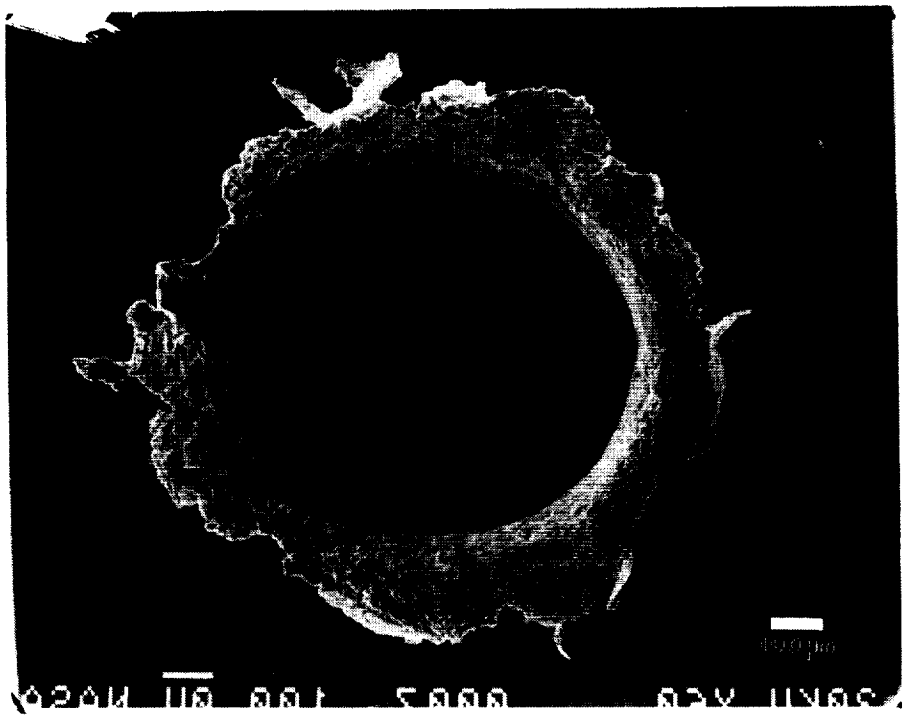

Figure 4.1 - Entry hole.

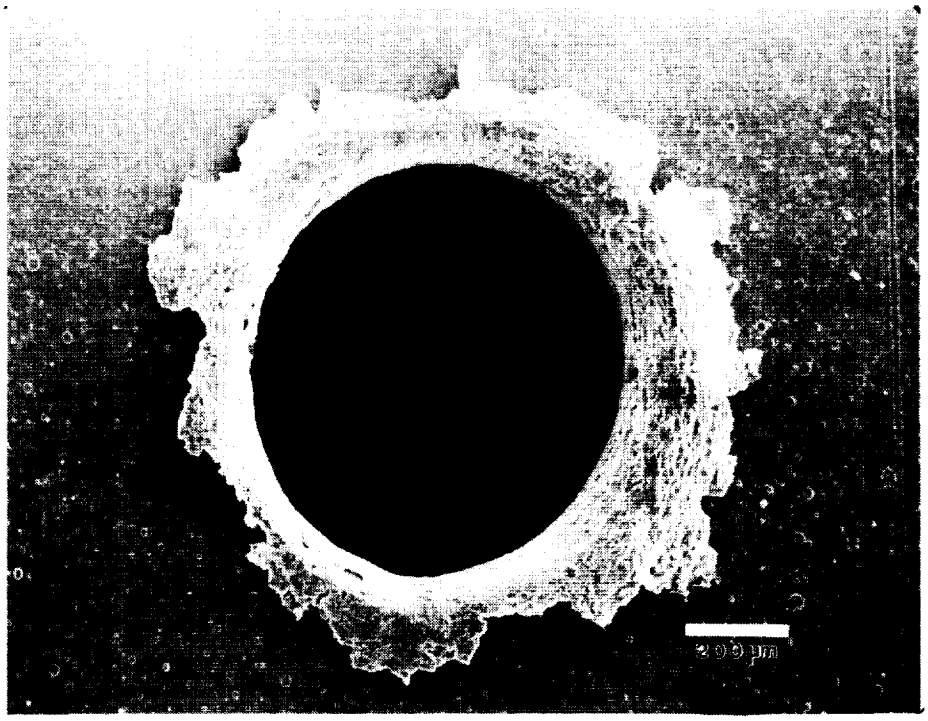

Figure 4.2 - Exit hole.

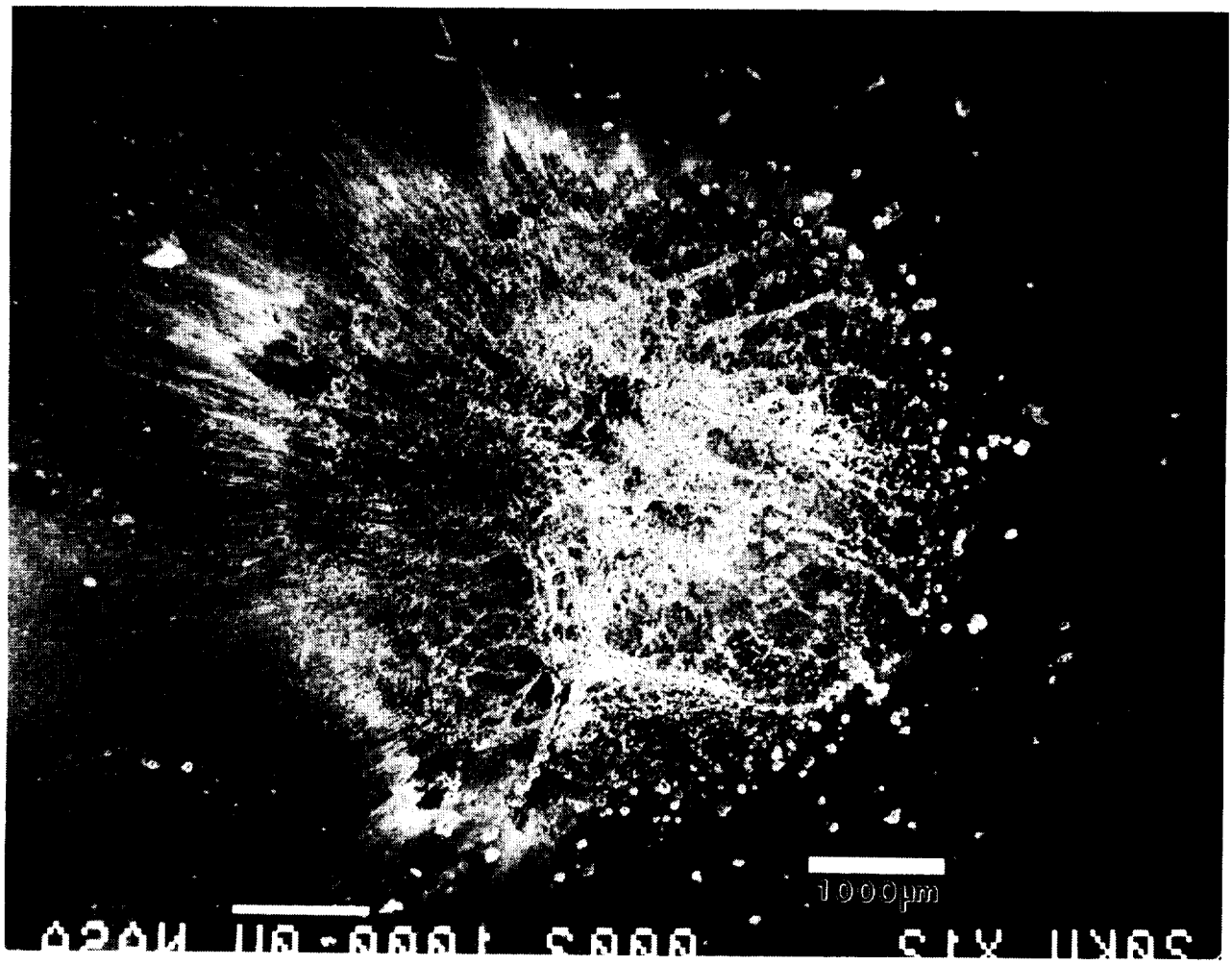

Figure 4.3 - Spray pattern.

Figure 5 shows the size distribution of holes in the aluminum louvers. Most of the holes are in the size range of 180 micrometers to 400 micrometers. Below 180 micrometers, impacts produced craters rather than holes in the 125-micrometer thick louver material. Also shown in this figure is the distribution between identified micrometeorite holes and identified orbital-debris holes. Orbital-debris holes clearly are a minority of the population in this size range. However, that is somewhat misleading. Orbital debris particles have a mean velocity relative to a satellite in low-Earth orbit of about 10 km/sec, but micrometeorites have a mean velocity of about 20 km/sec relative to the satellite. Therefore, debris particles of equal mass and density as micrometeorites are likely to make smaller holes or even craters rather than holes. Consequently, the difference between the abundance of micrometeorite holes and orbital debris holes does not accurately reflect the difference in flux between these two populations; the fluxes are more nearly equal than is indicated by the hole data.

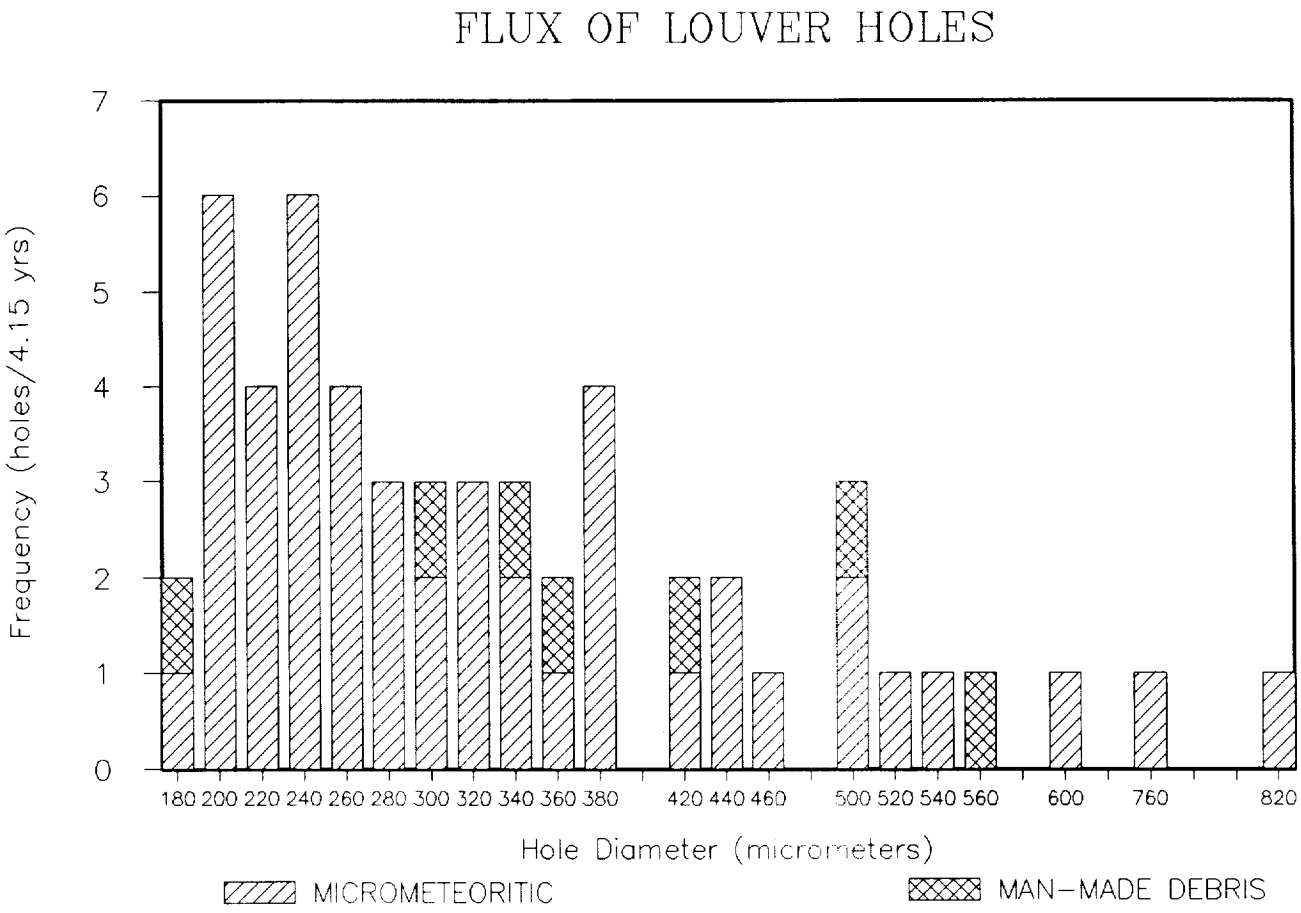

Figure 5

In Figure 6, the mass of the impacting projectile has been calculated using experimental penetration data on the louvers (Reference 1) and assumed velocities (approximately 20 km/sec for micrometeoroids, and approximately 10 km/sec for orbital-debris particles). Over most of the range, the projectile flux difference is only about a factor of three rather than the order of magnitude suggested by the hole data alone. At lower masses the two flux curves begin to diverge because the lower velocity debris microparticles are beginning to make craters rather than holes so that the flux dropoff is an artifact of the transition from holes to craters for these particles.

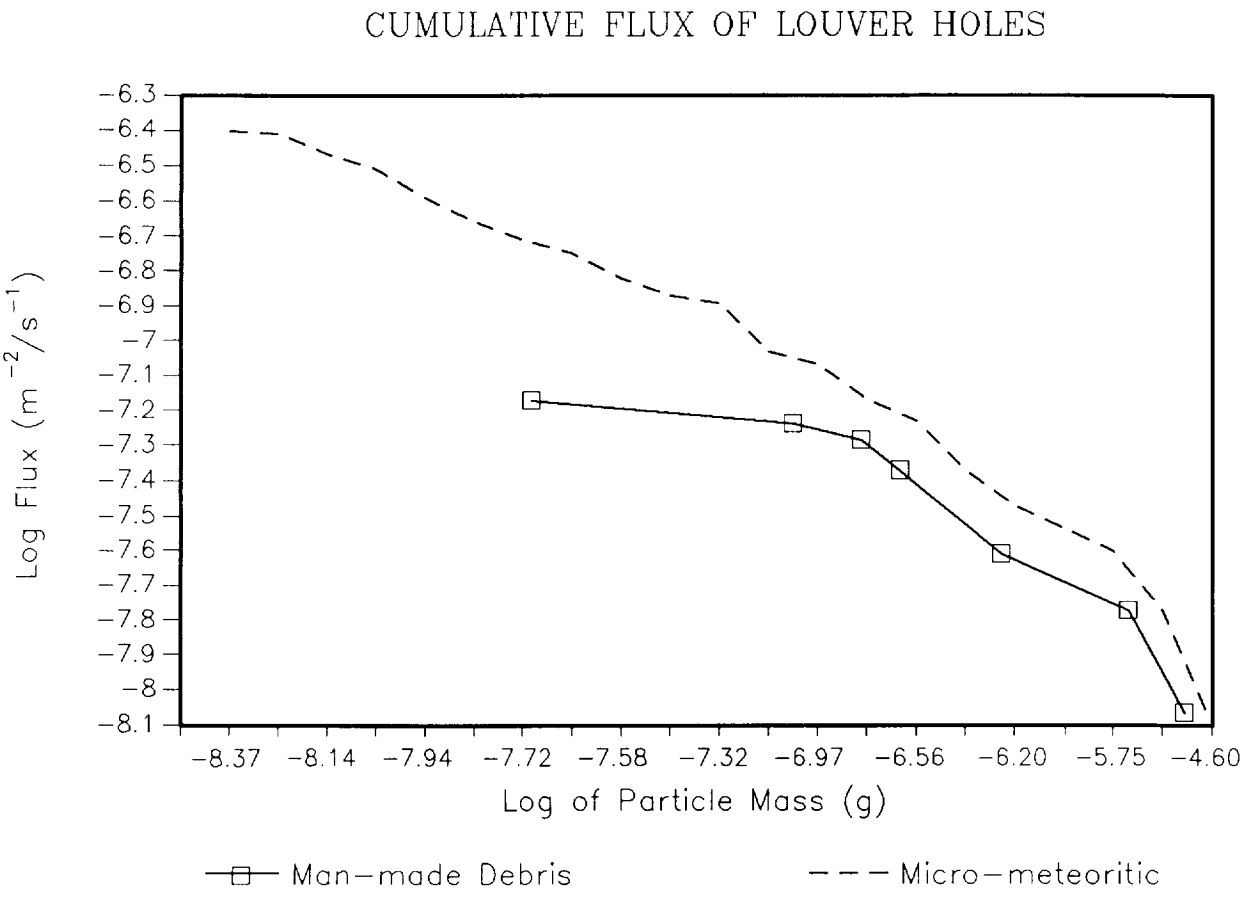

Figure 6

This diagram (Figure 7) of the louvers shows 15 areas which we selected for more detailed higher magnification study. In these selected areas we scanned the surfaces at a magnification of 10,000X designed to reveal all craters larger than 1 micrometer and, in selected subareas, all craters larger than 0.1 micrometer. The smallest observed crater was 50 nanometers in diameter. Examples of some of these craters are illustrated by Figures 7.1 - 7.5.

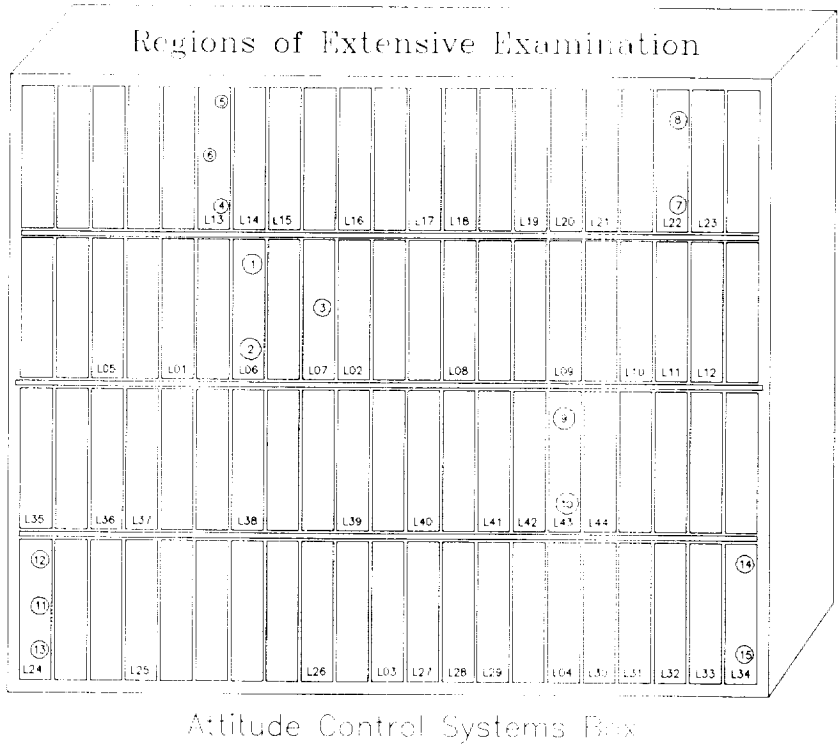

Figure 7

Example of Crater

Figure 7.1

Examples of Craters

Figure 7.2

Figure 7.3

Examples of Craters (cont.)

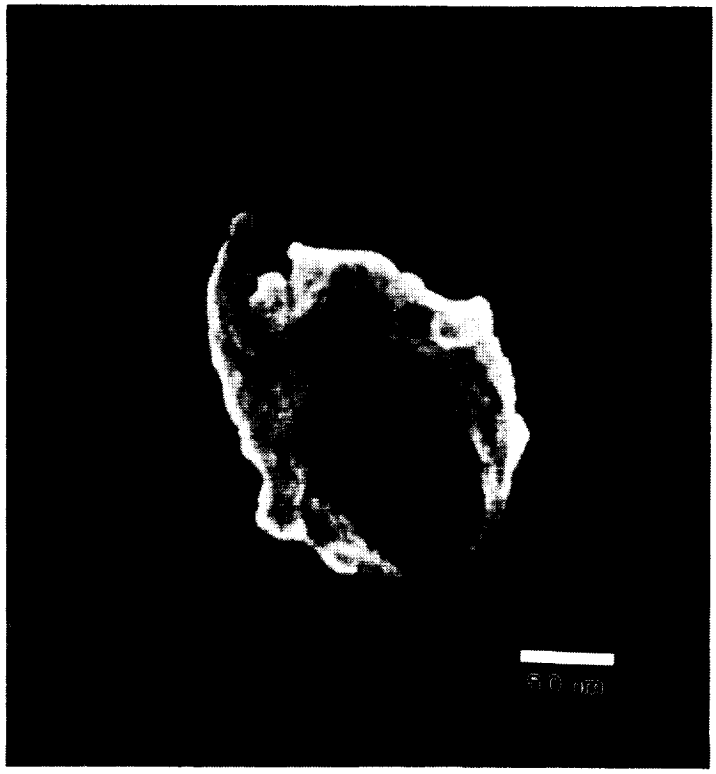

Figure 7.4

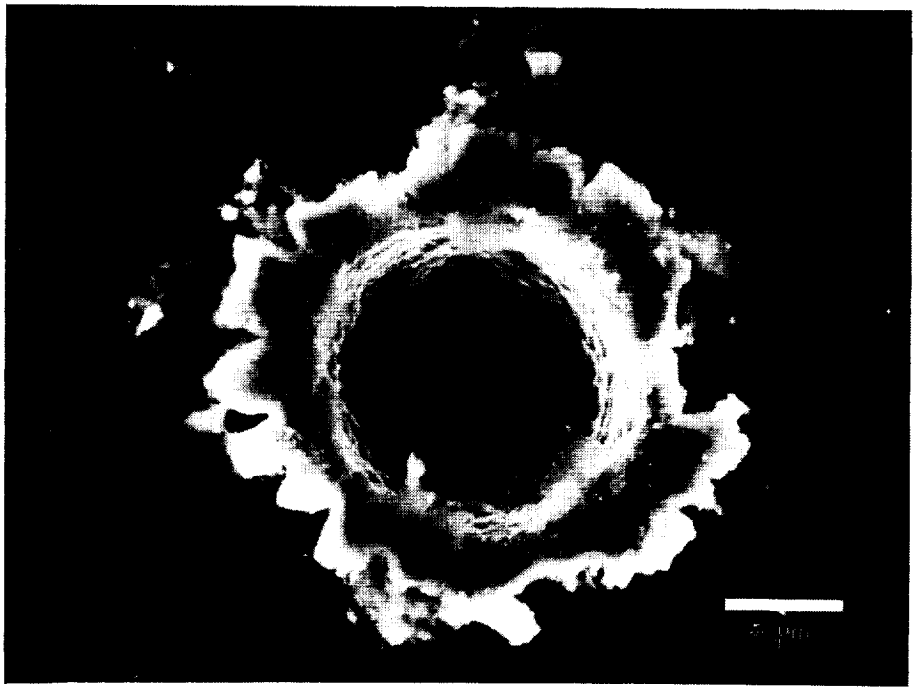

Figure 7.5

Figure 8 shows the abundance of small craters (0.1 - 0.5 micrometers) in several of the regions examined at high magnifications (Figure 7). The abundance of small craters are higher in regions 4, 5, and 6 compared to regions 9, 10, 14, and 15. Shielding calculations (Reference 2) show that regions 4, 5, and 6 have a higher proportion of the solid angle field of view obstructed by the nearby solar panel. This correlation would support an interpretation that many of these small impact craters are caused by high velocity secondary ejecta from primary impacts into the backside of the nearby solar panel while the smallest craters (less than 1 micrometer) do not contain enough detectable residue for chemical identification; the larger craters (5 - 100 micrometers) often contain detectable residue and many of these craters contain residue rich in titanium, oxygen, and sometimes zinc. These compositions are typical of pigments used in chemglaze paint on the solar panels and other parts of the spacecraft. Consequently, some of these impacts could be from secondary projectiles generated at other Solar Max surfaces, although other compositions including potassium and silicon-rich and aluminum oxide have originated on other spacecraft or from solid rocket exhaust.

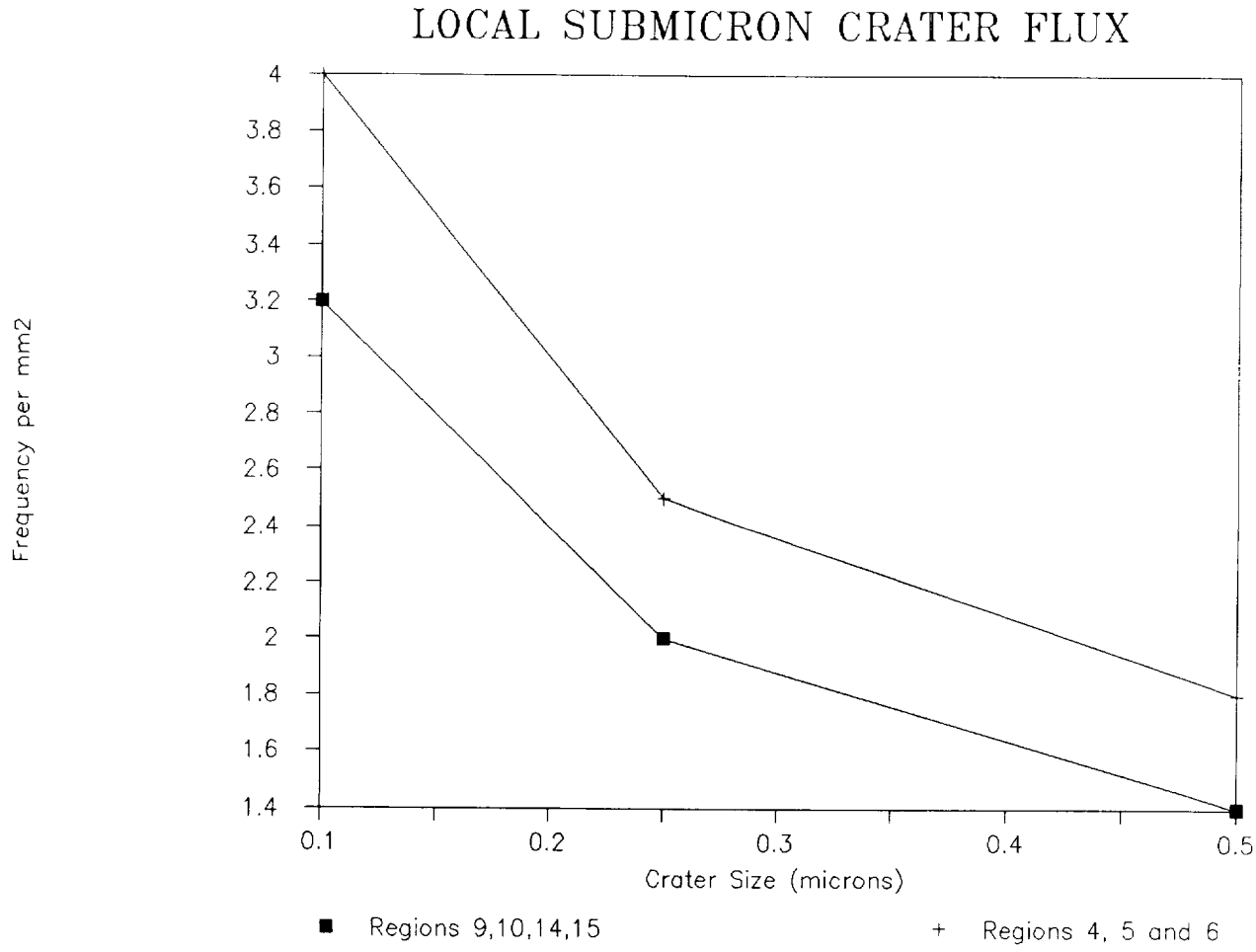

Figure 8

Figure 9 shows the abundance of adhering particulate contamination on the various examination regions of the aluminum louvers as shown in Figure 7. These particles are mostly titanium dioxide and are typically 0.2 - 0.5 micrometers in diameter. The particles occur individually and in clumps (Figure 9.1). Abundance of these particles is not random but increases systematically from regions 14 and 15 to regions 4, 5, and 6. As stated previously, regions 4, 5, and 6 shielding calculations have shown that regions 4, 5, and 6 have the largest solid angle field of view for the nearby solar panel. Consequently, we suggest that many of the surface particulates come from the solar panel and are in fact paint pigment particles. The particles are clean-appearing and lack the binder typical of unflown chemglaze paints. We suggest that the near-surface binder of this paint has been eaten away by atomic oxygen erosion and the included pigment particles have been released by thermal cycling or other mechanisms and have drifted to the louvers and have been deposited on their surfaces. Self-contamination from released paint pigment may be a widespread particulate contamination on other spacecraft.

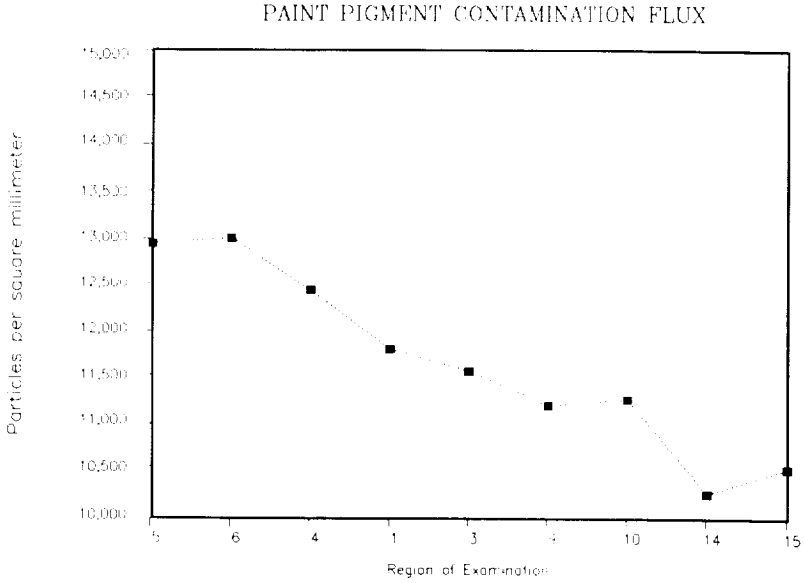

Figure 9

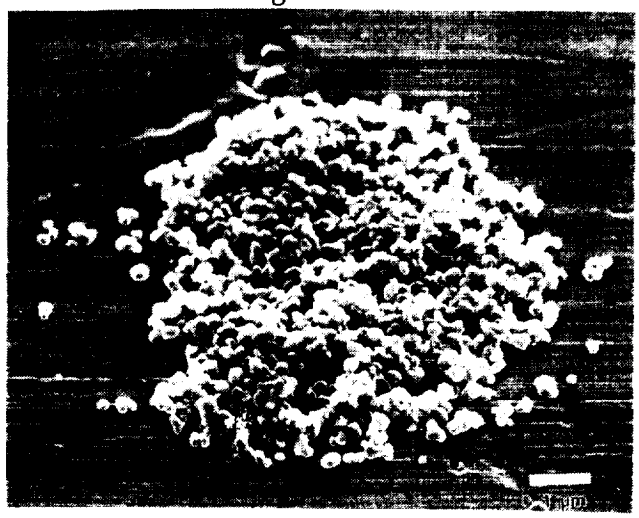

Example of adhering particulate contamination

Figure 9.1

Figure 10 shows the overall flux of holes and craters on the aluminum louvers over the size range from 10 micrometers to 1 millimeter. For the size region dominated by holes, the micrometeorite curve is clearly higher than the orbital-debris curve as discussed previously (Figures 4 and 5). The transition region between holes and craters is clearly shown in the region around 200 micrometers. While not shown on this figure, chemical data indicate that a high proportion of the smaller craters are formed by debris projectiles rather than micrometeorites. Therefore, the flux curves must cross over, probably in the crater region between 50 and 100 micrometers. As pointed out elsewhere in this report, the population of large (centimeters to meters) projectiles is dominated by orbital debris. Thus, based on Solar Max results, small projectiles (approximately those which make less than 50 micrometers crater diameters on aluminum) are dominated by orbital debris (mainly paint pigments with lessor aluminum oxide solid rocket exhaust), the larger projectiles (centimeters to meters) are dominated by orbital debris, and only the narrow region between (projectiles making holes or craters in aluminum from about 0.1 mm to possibly 1 cm) is still dominated by natural meteoroids.

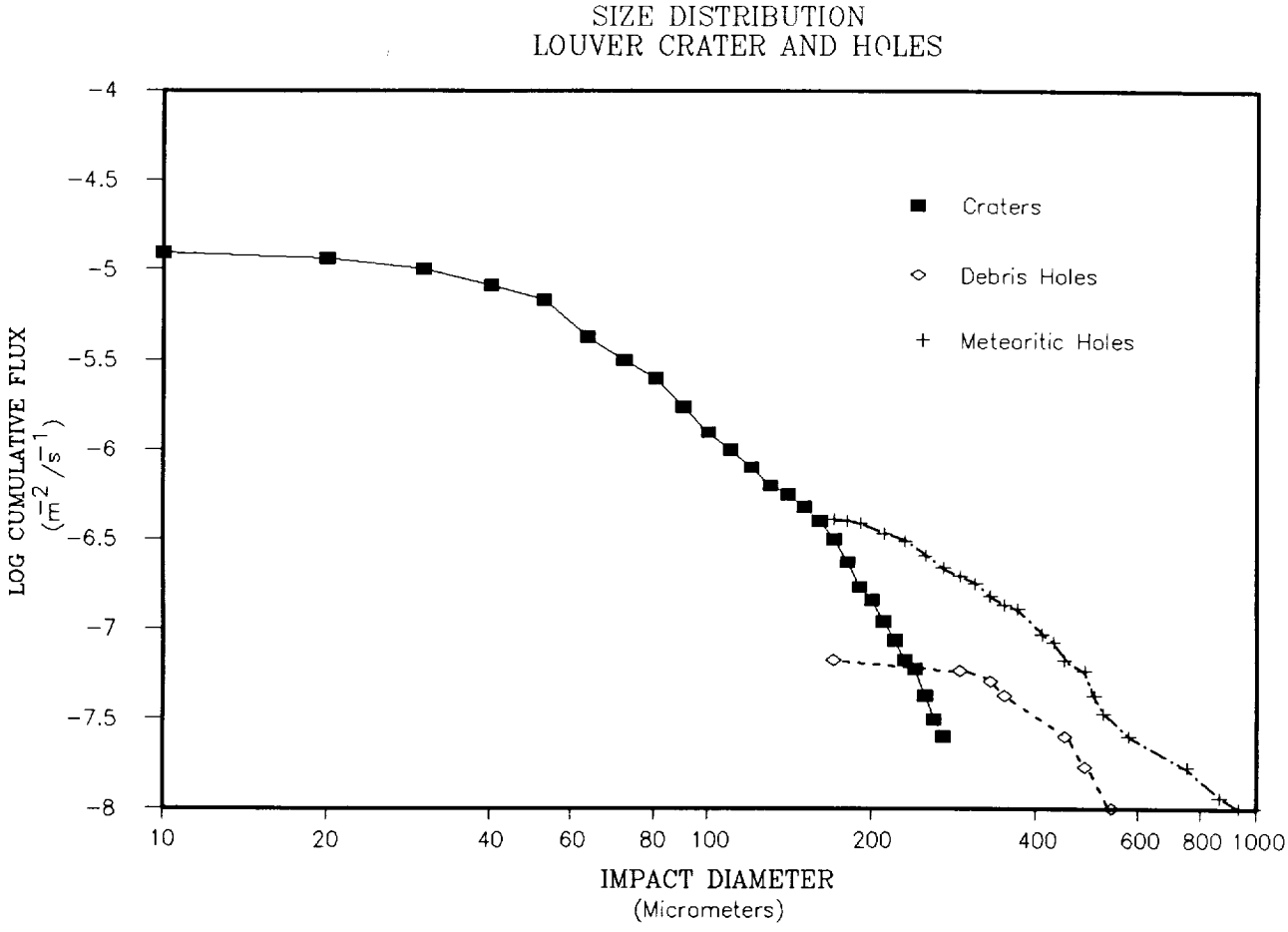

Figure 10

Figure 11 shows some of the major conclusions which have emerged from the study of Solar Maximum space-exposed surfaces having more than four years exposure to micrometeorites, atomic oxygen erosion, and orbital debris microparticle abrasion.

CONCLUSIONS

1. On Solar Max louvers, the flux of micrometeoritic holes is three times greater than orbital debris holes.

2. The majority of smaller impacts (< 20um in diameter) are produced by man-man debris projectiles.

3. A significant proportion of the smallest impacts are caused by secondary ejecta originating from the solar panel.

4. Low velocity projectiles (particles and clusters of paint pigments) are abundant. These most likely originate from the nearby solar panel.

5. Atomic oxygen erosion is a contributing factor to low velocity surface contamination.

6. Hardware exposed to space will be impacted by a broad mass range of both micrometeorite and orbital debris projectiles and may be further degraded by atomic oxygen erosion and effects of secondary ejecta.

Figure 11

Figure 12 shows the outline of a Shuttle experiment of material abrasion by solid rocket exhaust particles.

SHUTTLE WITNESS PLATE RESULTS

PURPOSE

DETECT IMPACTS FROM PAM D2 SOLID ROCKET MOTOR

DETERMINE FLUX AND SIZE DISTRIBUTION OF PARTICLES

DETERMINE ABRASION EFFECTS ON VARIOUS

CONDITIONS

PAM D2 ROCKET WAS 17 KM FROM SHUTTLE ORBITER

BURN DURATION WAS 96 SECONDS

RESULTS

ALUMINUM SURFACES

COPPER SURFACES

STAINLESS STEEL SURFACES

INCONEL SURFACES

QUARTZ GLASS SURFACES

Figure 12

Figure 13 shows the ratio between the diameter of the retained aluminum oxide projectile and the diameter of the resulting crater or pit in the stainless steel (15-5) witness plate. This witness plate retained 62% of the impacting projectiles. The mean projectile/pit diameter for stainless steel is 0.90 $\pm$ 0.09. Figure 13.1 illustrates a fractured SRM projectile in a stainless steel target.

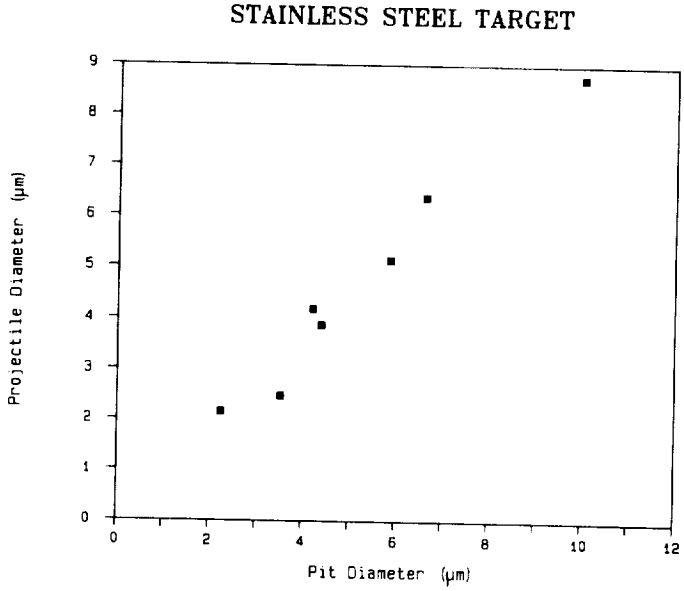

Figure 13

Fractured SRM projectile in a stainless steel target

Figure 13.1

Figure 14 shows the projectile to pit ratios for the inconel target from the Shuttle Orbiter witness plate experiment. The mean projectile/pit diameter for this target is 0.9 $\pm$ 0.09. The inconel target retained 48% of the impacting aluminum oxide particles, the least of any of the targets.

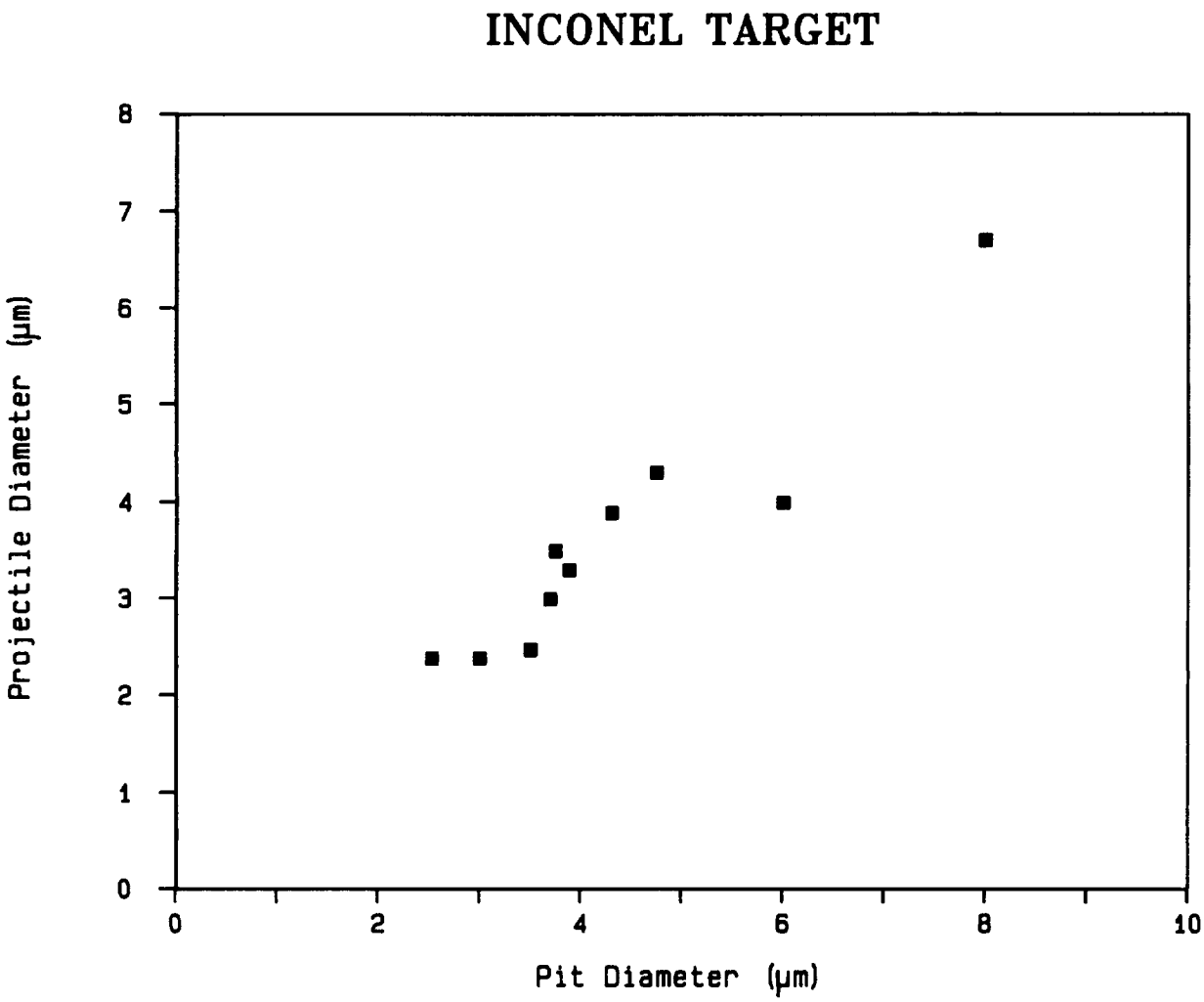

Figure 14

Shuttle witness plate impact results on scanned areas of the copper, aluminum, and quartz glass targets. The abundance of impacts per unit area is statistically equivalent for the three targets. The mean number of impacts for all pits greater than 1 micrometer in diameter is 10.25/mm^2. If pits smaller than 1 micrometer are included, the mean impact abundance for all size ranges and all targets is 15.4 impacts/mm^2, (Table 1).

Table 1

MEAN IMPACTS/mm^2 RANGING FROM 1 um TO >10 um IN DIAMETER FOR ALL TARGETS

TARGET	TOTAL IMPACTS	SURFACE AREA SCANNED (mm^2)	IMPACTS/mm^2
COPPER	111 +/- 10.34	9.88	11.2 +/- 1.05
ALUMINUM	63 +/- 7.94	6.37	10.0 +/- 1.25
QUARTZ	23 +/- 4.80	2.97	7.7 +/- 1.61
Total	197	19.22	

MEAN IMPACTS/mm^2 = 197/19.22 = 10.25

Figure 15 shows the relationship between measured depth/diameter ratios for a number of pits (lacking retained projectiles) and the calculated impact velocity. An emperically determined relationship between stereometically measured pit depth and projectile diameter is used (Hermann & Jones, 1962), Reference 3.

$$P/d = K_1 \times \mathrm{Ln}\ (1 + K2V^2)$$

where
- P = depth of penetration
- d = diameter of projectile
- K_1 = 0.604, constant determined for aluminum projectile and target
- K2 = 0.593, constant determined for aluminum projectile and target
- V = velocity (km/s)

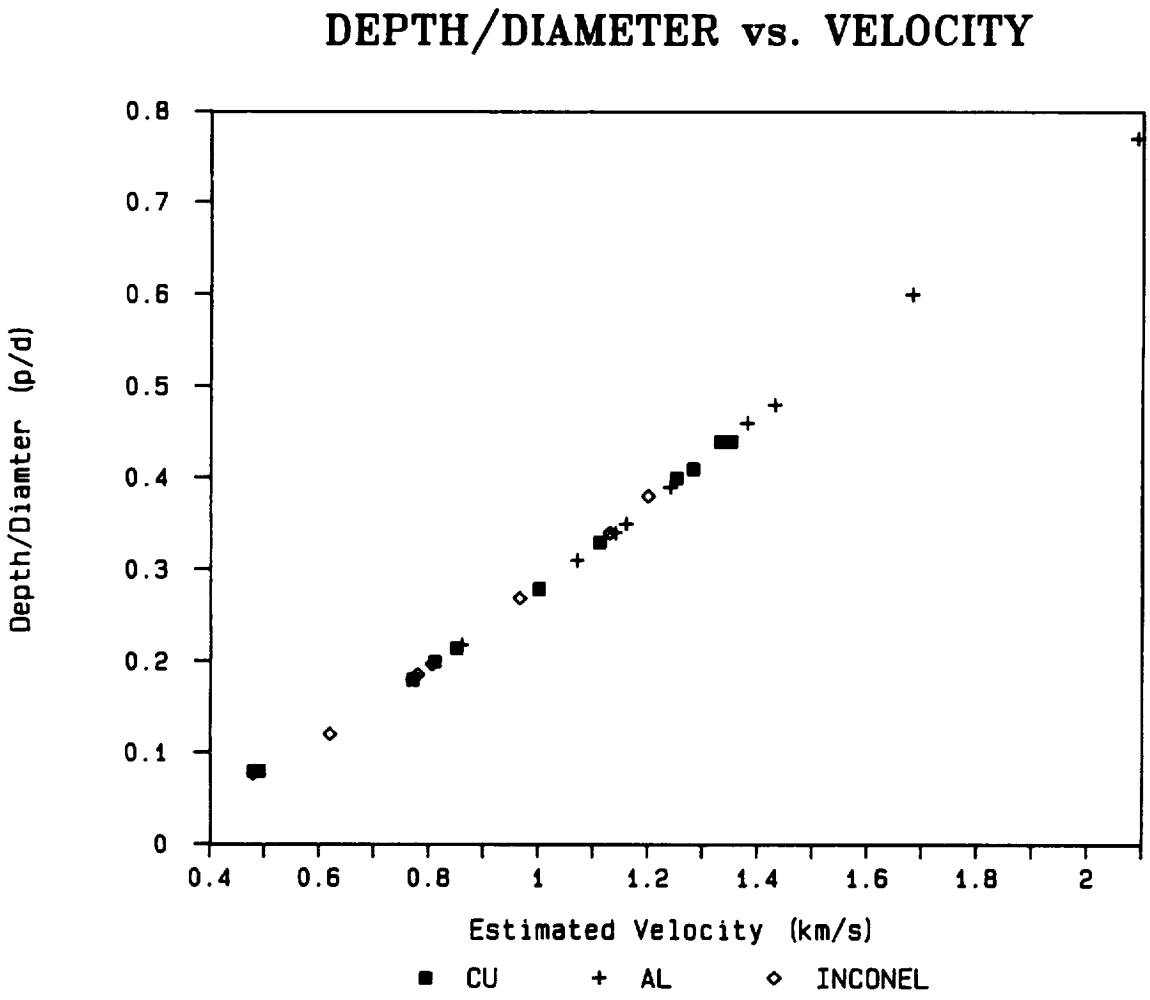

Figure 15

The size distribution of aluminum oxide particles impacting targets on the Shuttle Orbiter witness plate experiment is shown in Table 2. This distribution is strongly peaked at 1 to 5 micrometers. The smallest pit observed was 0.8 micrometers in diameter and the largest pit observed was 14 micrometers.

Table 2

SIZE DISTRIBUTION FOR IMPACT FEATURES

TARGET	SIZE RANGE (um)				TOTAL IMPACTS
	<1	1-5	6-10	>10	
Copper	69	105	6	0	180
Aluminum	20	57	6	0	83
Quartz*	10	21	1	1	33
Total	99	183	13	1	296
DISTRIBUTION BY SIZE (%) (All Targets)	33.4	61.8	4.4	0.34	

*Dimension refers to pit diameter, not spall diameter

Table 3 shows the calculated eroded area for metal targets (aluminum, copper, stainless steel, and inconel). The calculations show that approximately 0.01% of the surfaces were eroded or destroyed by impingement of particles from the plume of the solid rocket.

Table 3

PERCENTAGE OF SURFACE AREA EROSION ON METALLIC TARGETS

Diameter Range (um)	Average Diameter (um)	Average Radius (um)	Surface Area Eroded Impact (mm^2)[1]
<1	0.9*	0.4	6.4E-7
1-5	3.0	1.5	7.1E-6
6-10	8.0	4.0	5.0E-5
>10	12.0**	6.0	1.1E-4

Surface Area Eroded/Impact x Average Impact Density[2] x Size Frequency[3] x Total Surface Area = Surface Area Eroded (mm^2)

6.4E-7 mm^2 x 15.2/mm^2 x 0.339 x 3354.3 mm^2 = 0.011
7.1E-6 mm^2 x 15.2/mm^2 x 0.613 x 3354.3 mm^2 = 0.221
5.0E-5 mm^2 x 15.2/mm^2 x 0.0445 x 3354.3 mm^2 = 0.114
1.1E-4 mm^2 x 15.2/mm^2 x 0.0034 x 3354.3 mm^2 = 0.020
Total Surface Area Eroded (mm^2) = 0.366

Total Metallic Surface Area Exposed to the Plume = 3354.3 mm^2

Area Eroded (%) = 0.366/3354.3 x 100 = 0.011

*Smallest observed size was approximately 0.8 um
**Largest observed size was approximately 14.0 um
[1]Approximate Surface Area Eroded/Impact = sphere = $3.14159r^2$
[2]Table 2
[3]Table 1

Table 4 shows the calculated eroded area for the quartz glass target. The calculations show that approximately 0.34% of the glass surface was eroded or destroyed by the particle impacts. This area is more than 30 times that for the metal surfaces subjected to the same flux of aluminum oxide particles.

Table 4

PERCENTAGE OF SURFACE AREA EROSION ON NON-METALLIC TARGETS

Pit Diameter Range (um)	Ave. Pit Diameter (um)	Ave. Pit Radius (um)	Ave. Spall to Pit Ratio[1]	Ave. Spall Radius (um)
<1	0.9*	0.4	1/5.55	2.5
1-5	3.0	1.5	1/5.55	8.3
6-10	8.0	4.0	1/5.55	22.2
>10	12.0**	6.0	1/5.55	33.3

Surface Area Eroded/ Impact (mm^2)[2]
1.96E-5
2.18E-4
1.55E-3
3.48E-3

Surface Area Eroded/Impact x Average Impact Density[3] x Size Frequency[4] x Total Surface Area = Surface Area Eroded (mm^2)

$1.96E\text{-}5\ mm^2 \times 15.2/mm^2 \times 0.339 \times 1570.5\ mm^2 = 0.159$
$2.18E\text{-}4\ mm^2 \times 15.2/mm^2 \times 0.613 \times 1570.5\ mm^2 = 3.190$
$1.55E\text{-}3\ mm^2 \times 15.2/mm^2 \times 0.0445 \times 1570.5\ mm^2 = 1.646$
$3.48E\text{-}3\ mm^2 \times 15.2/mm^2 \times 0.0034 \times 1570.5\ mm^2 = 0.283$

Total Surface Area Eroded (mm^2) = 5.278

Total Non-Metallic Surface Area Exposed to the Plume = 1570.5 mm^2

Area Eroded (%) = 5.278/1570.5 x 100 = 0.336

*Smallest observed size was approximately 0.8 um
**Largest observed size was approximately 14.0 um
[1]Table 8
[2]Approximate Surface Area Eroded/Impact = sphere = $3.14159r^2$
[3]Table 2
[4]Table 1

Figure 16 shows modeled orbital decay times and settling times (after reaching zero horizontal velocity) for small particles. For example, a 0.5 micrometer (radius) particle released from a spacecraft at 500 km altitude will lose all of its orbital velocity in 2.2 hours as a result of air drag. During this time the particle loses altitude to about 380 kilometers. The particle then falls or settles over 6.8 more hours to the stratosphere below 100 km where the particle slows down considerably as it encounters significant air. Equation used for orbital decay is from Mueller (1981) Reference 4 and equation used for settling times is from R. Reynolds (1987), (Lockheed, JSC), [personal communication].

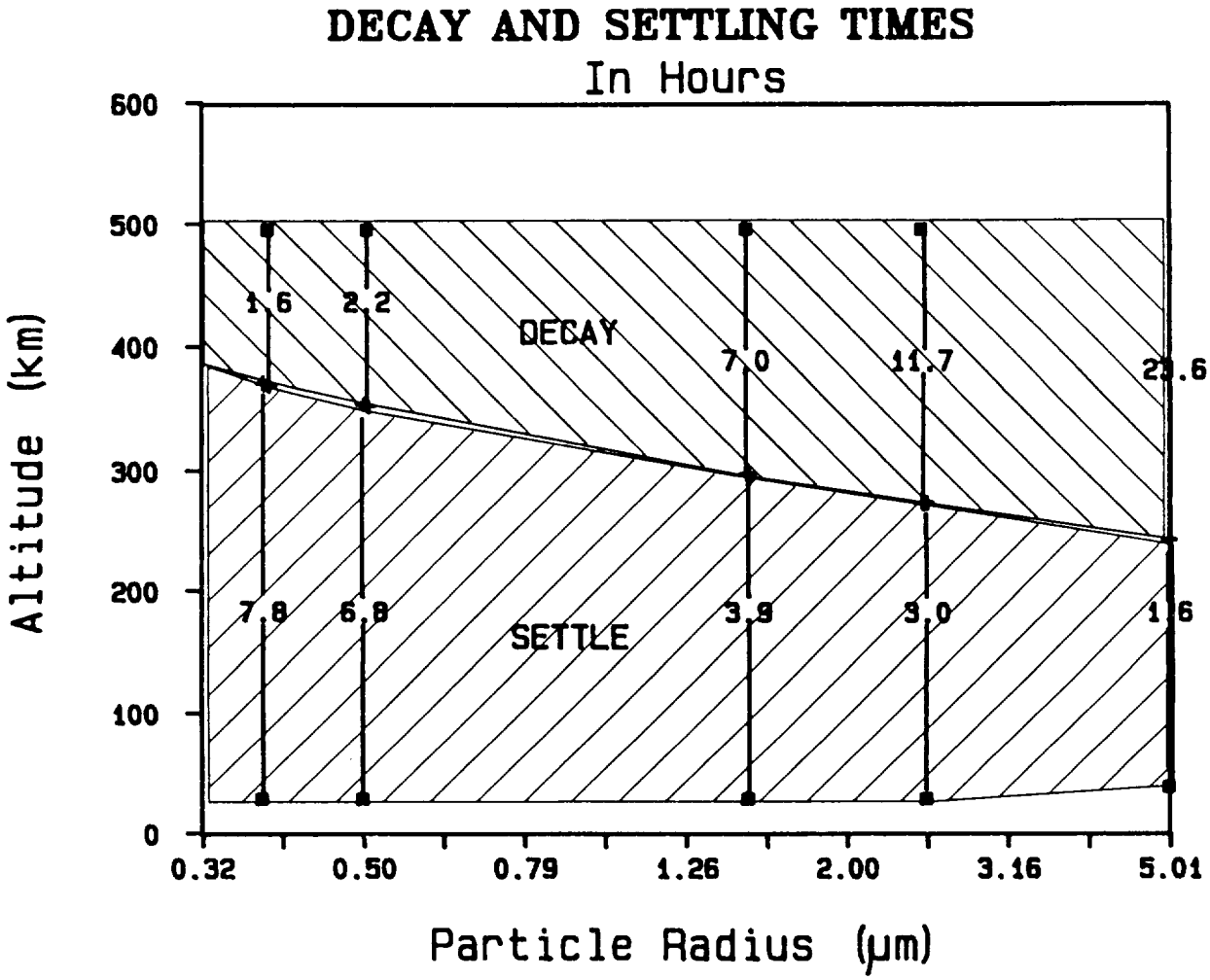

Figure 16

Figure 17 (Zolensky et aL, 1988, Reference 5) shows measured abundance for aluminum-rich stratospheric dust particles in the stratosphere as collected by the NASA cosmic dust collection program. Most of these aluminum-rich particles are interpreted to be from spacecraft and rockets. The abundance of these spacecraft-derived particles increased more than an order of magnitude between 1981 and 1984, the most recently analyzed sample. Additional analysis of existing samples is needed to determine if the abundance of these particles is still increasing. Recent (June 1988) deployment of the large area collectors will greatly increase the amount of sampled stratospheric dust available for analysis.

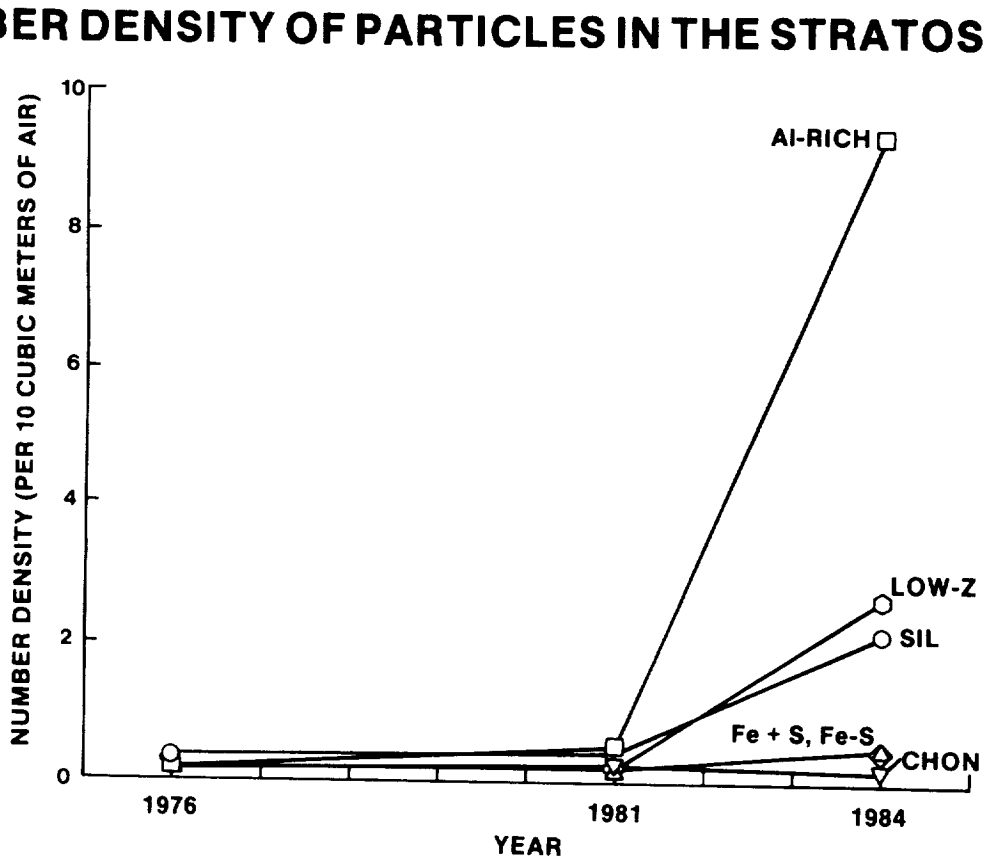

Figure 17

REFERENCES

1. Carey, W. C.: Properties and Interactions of Interplanetary Dust, pp. 131-136, 1985.

2. Warren, J.: Optical Observations of Impact Features on Solar Max Thermal Blankets and Louvers. Lunar and Planetary Science XIX, 1988.

3. Hermann, W.: Correlation of Hypervelocity Impact Data. Proceedings of the Fifth Symposium of Hypervelocity Impact (Colorado), #G-0020-62, Vol. 1, Part 2, 1962.

4. Mueller, A. C.: The Decay of the Low Earth Satellite for the Orbital Debris Study. J. O. 69-067, Lockheed 17520, 1981.

5. Zolensky, M. E.: Stratospheric Particle Abundance and Variations Over the Last Decade. Lunar and Planetary Science Conference XVII, pp. 969-970, 1986.